Dissociative photodetachment studies of $O^-(H_2O)_2$, $OH^-(H_2O)_2$, and the deuterated isotopomers: Energetics and three-body dissociation dynamics

Todd G. Clements, A. Khai Luong, Hans-Jürgen Deyerl, and Robert E. Continetti
Department of Chemistry and Biochemistry, University of California, San Diego, 9500 Gilman Drive, La Jolla, California 92093-0314

Photoelectron–photofragment coincidence spectroscopy was used to study dissociative photodetachment of the doubly hydrated clusters of oxide and hydroxide, $M^-(H_2O)_2 \rightarrow M + 2H_2O + e^-$ (M=O, OH). These experiments yield information on the energetics of the parent anion and the dissociation dynamics of the photodetached neutral species. Photoelectron spectra and photoelectron–photofragment coincidence spectra are presented and compared to data for $O^-(H_2O)$ and $OH^-(H_2O)$. Unlike the singly hydrated species, no evidence of vibrationally resolved product translational energy distributions is observed. The second hydration energy of O^- with both H_2O and D_2O was also measured to be 0.80 ± 0.08 and 0.81 ± 0.08 eV, respectively. The three-body dissociation dynamics of the neutral clusters produced by photodetachment were studied by measuring the velocities and recoil angles of all the particles in coincidence. The observed partitioning of momentum is consistent with a two-step mechanism or dissociation from a wide range of starting geometries. © *2001 American Institute of Physics.* [DOI: 10.1063/1.1366332]

I. INTRODUCTION

Hydrated neutral and ionic clusters are known to be important participants in the chemistry of the atmosphere[1–4] and are also present in combustion processes.[5] Specifically, reactions of O^- and OH^- and the corresponding neutral species O and OH with a single water molecule have received considerable attention in the literature due to their importance in combustion and atmospheric models.[6–10] The small size of these clusters also makes them amenable to high-level theoretical studies.[11–13] Data on these clusters with two or more waters may provide insights into bulk solvation phenomena.[14,15] Additionally, three-body association reactions of hydroxide and oxide with water are possibly important reactions in the lower ionosphere.[16] Photoelectron–photofragment coincidence (PPC) spectroscopy is a useful method for studying the energetics and dissociative photodetachment dynamics of small anionic clusters,[17,18] and provides an approach to studying the three-body dynamics of the neutral complexes produced by photodetachment of the anions. In this paper, PPC spectroscopy is applied to $O^-(H_2O)_2$, $OH^-(H_2O)_2$, and the deuterated analogs to probe the energetics and three-body dynamics of these systems.

Previous experimental studies on the hydrates of the oxide anion, $O^-(H_2O)_n (n \geq 1)$, have focused on reaction rate constants with a variety of small molecules.[19–26] There have been few theoretical studies on the structure and energetics of oxide bound to two or more waters. Using density functional theory (DFT) with a double zeta basis set including polarization functions (DZVP2),[27,28] Schindler *et al.* proposed that the $O^-(H_2O)_2$ cluster is composed of an L-shaped dimer of hydroxide moieties solvated on one end by the additional water molecule,[24] as seen in Fig. 1(a). Both this

structure and one composed of a central oxide symmetrically bound to two waters [Fig. 1(b)] imply that there may be two low energy dissociative photodetachment (DPD) channels for this species,

$$O^-(H_2O)_2 \rightarrow O + H_2O + H_2O + e^-, \quad (1)$$

$$O^-(H_2O)_2 \rightarrow OH + OH + H_2O + e^-. \quad (2)$$
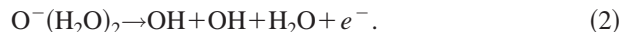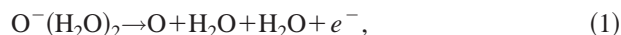
Schindler *et al.* calculated an incremental second hydration/dissociation enthalpy ($\Delta H^{hyd}_{298 K,1\leftarrow2}(O^-)$) of 0.83 eV,[24] defined to be the enthalpy required to remove the second water molecule from $O^-(H_2O)_2$ according to the reaction $O^-(H_2O)_2 \rightarrow O^-(H_2O) + H_2O$. The only other reported $\Delta H^{hyd}_{298 K,1\leftarrow2}(O^-)$ is the range 0.65–0.87 eV, based on the energetics of $OH^-(H_2O)_n$.[19] These enthalpies are smaller than those for addition of the first water to oxide which are in the range 1.08–1.55 eV.[19,22,24] Deyerl *et al.* have recently determined $\Delta E^{hyd}_{0 K,0\leftarrow1}(O^-) = 1.15$ eV using PPC spectroscopy.[29]

The body of work available on $OH^-(H_2O)_n$ is considerably larger. A number of studies have been performed on the rates of $OH^-(H_2O)_n$ reactions with small molecules.[16,20,21,23,30,31] Complementing these experiments are a number of theoretical studies of the structure and energetics of $OH^-(H_2O)_n$.[32–39] Efforts have also been made to provide a link between small cluster data and bulk aqueous solvation.[15,40,41] The most likely structure of $OH^-(H_2O)_2$ has a central OH^- solvated to two waters via hydrogen bonds in a bent, almost planar configuration[34] as shown in Fig. 1(c). Experimental values of $\Delta H^{hyd}_{298 K,1\leftarrow2}(OH^-)$ have been measured in the range of 0.71–0.78 eV,[19,42–44] while most recent theoretical values lie in the range 0.81–0.89 eV.[15,34,36,38,41] As with O^-, $\Delta H^{hyd}_{298 K,1\leftarrow2}(OH^-)$ is smaller than

8436

J. Chem. Phys., Vol. 114, No. 19, 15 May 2001

Studies of O⁻(H₂O)₂, OH⁻(H₂O)₂   8437
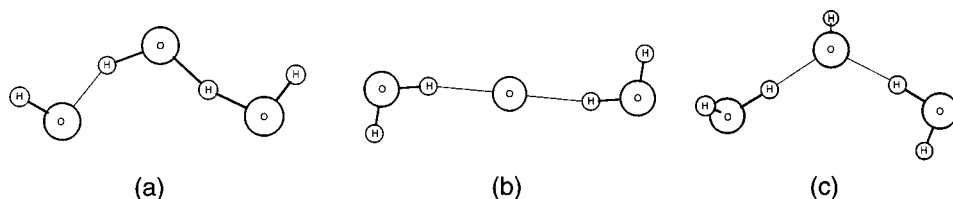
FIG. 1. *Ab initio* geometries for (a) $O^-(H_2O)_2$ (Ref. 24); (b) $O^-(H_2O)_2$ (UHF/6-311++G**), and (c) $OH^-(H_2O)_2$ (Ref. 34).

$\Delta H^{hyd}_{298 K, 0 \leftarrow 1}(OH^-)$, with the most recent experimental values of the latter quantity centered around 1.16 eV.[13,19,32–34,36,41–45] For this cluster, the only low energy dissociative photodetachment pathway is

$$OH^-(H_2O)_2 \rightarrow OH + H_2O + H_2O + e^-. \quad (3)$$

Despite the large body of work available on these systems, there are still questions that remain to be answered. There have been no studies of the three-body association or dissociation dynamics of either the ionic clusters or the neutrals produced by photodetachment. In addition, there are no previous measurements of $\Delta H^{hyd}_{1 \leftarrow 2}(O^-)$, nor have photoelectron spectra for the doubly hydrated clusters been reported. This paper presents photoelectron spectra, photoelectron–photofragment kinetic energy correlation spectra, total energy spectra, and incremental hydration/dissociation energies for $O^-(H_2O)_2$, $OH^-(H_2O)_2$, and the deuterated analogs. The three-body dissociation dynamics of the neutral clusters are discussed in terms of the observed momentum partitioning.

II. EXPERIMENT

The experimental technique has been previously described in detail and will only be briefly reviewed here.[46,47] PPC spectroscopy is carried out by intersecting a fast (4 keV) negative ion beam with a linearly polarized laser beam. Photodetached electrons and neutral photofragments are then detected in coincidence, allowing complete kinematic characterization of three-body dissociations.

Ions were produced by intersecting a 1 keV electron beam with a continuous supersonic expansion of the source gas through a 50 μm aperture. A pulsed beam running at 1 kHz yielded equivalent results, but the continuous source was employed owing to higher ion intensities for the ions of interest. The source gas for O^- clusters was 15% N_2O, 25% Ne, and 60% He, while for OH^- clusters an expansion of 8% N_2O in methane was used. In both cases the gas was passed over H_2O or D_2O at room temperature to form the hydrated clusters.

The continuous ion beam was accelerated and re-referenced to ground potential by a high-voltage switch run at a 1 kHz repetition rate. The ions were mass-selected by time-of-flight and guided into the interaction region where they were photodetached by the linearly polarized third harmonic (258 nm, 4.80 eV, 1.2 ps FWHM) of the regeneratively amplified output of a Ti:Sapphire laser (Clark CPA-2000). In these experiments, the linear polarization of the laser was fixed along the ion beam, parallel to the face of the electron detectors. The laser beam was focused to a 0.5 mm diameter spot at the interaction region, providing a fluence of approximately 5–10 mJ/cm² per pulse.

Photodetached electrons were detected by one of two opposed time- and position-sensitive electron detectors perpendicular to the ion and laser beams. Due to the use of a fast ion beam and the large solid angle of acceptance of the detector, the photoelectron laboratory energy was subject to Doppler broadening. Using the time- and position-of-arrival data to make the kinematic correction for the fast ion beam, the center-of-mass (CM) frame photoelectron kinetic energy (eKE) was obtained with a resolution of $\Delta E/E \sim 5\%$ at 1.3 eV.[47]

Neutral photofragments recoiled out of the fast ion beam over a 104 cm flight path and impinged on a microchannel-plate-based time- and position-sensitive multiparticle detector. The detector anode was composed of four independent crossed-delay-line quadrants, each of which is capable of detecting two particles per event. The number of neutral particles analyzed was selected by gating on the total charge observed, which is well-resolved for one, two, and three neutral particles. If an ideal parent beam is centered on the detector, momentum conservation dictates that no more than two particles will hit a given quadrant in a three-body dissociation. Monte Carlo simulation shows that for the current systems, approximately 5% of valid events were not detected due to effects from the 10 ns dead time on each quadrant, the spatial and temporal resolution, and the finite beam size. The affected events are at low kinetic energy release (KER), with significant discrimination below 0.04 eV and essentially zero discrimination above 0.08 eV. This detector has been shown to yield a photofragment translational energy resolution of $\sim 15\% \ \Delta E/E$ at 0.7 eV using the photodissociation of O_2^- at 258 nm, and effectively has no dead area within the active region.[46]

Kinematic analysis of dissociation events is straightforward since the three-dimensional recoil velocities of all three particles are measured directly. Details of the three-body data analysis were described in previous papers.[18,46] Briefly, for each event a CM reference frame is adopted with the largest particle recoil vector as the positive x-axis and the other two recoil vectors lying in the xy-plane. Conservation of mass and momentum is used to calculate the mass of each particle, with an uncertainty dictated by the distribution of CM (ion beam) velocity vectors. Once these masses are calculated, each particle is assigned a mass given the assumed dissociation pathway by minimizing the root-mean-squared error between the set of calculated fragment masses and the possible set of product masses. The recoil velocities and the assigned masses are used to calculate the CM translational
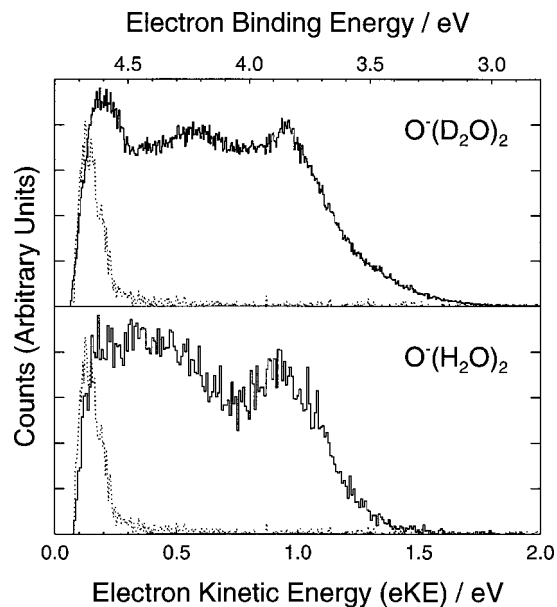
FIG. 2. Photoelectron spectra, $N(\text{eKE})$, of $O^-(H_2O)_2$ and $O^-(D_2O)_2$ at 4.8 eV.

FIG. 4. Photoelectron–photofragment kinetic energy correlation spectrum for $O^-(D_2O)_2$ at 4.8 eV. The contours represent the number of events with a given correlated value of E_T and eKE, $N(E_T,\text{eKE})$. The diagonal lines drawn represent the maximum translational energy, KE_{MAX}, available to the product channels (I) $O(^3P)+2D_2O+e^-$ and (II) $2OD+D_2O+e^-$.

energy release (E_T) for the three-body dissociation, given by the sum of the contributions from each particle. Examining two-particle charge-gated events, the data shows no evidence of two-body dissociative photodetachment for any of the systems. Therefore, all data presented are for three-body dissociations. The photofragment mass resolution of $m/\Delta m \approx 2.5$ at mass 32 amu (Ref. 46) does not allow the O, OH, and H_2O products to be distinguished.

III. RESULTS

Figure 2 shows the photoelectron spectra obtained for $O^-(H_2O)_2$ and $O^-(D_2O)_2$. Figure 3 shows the $OH^-(H_2O)_2$
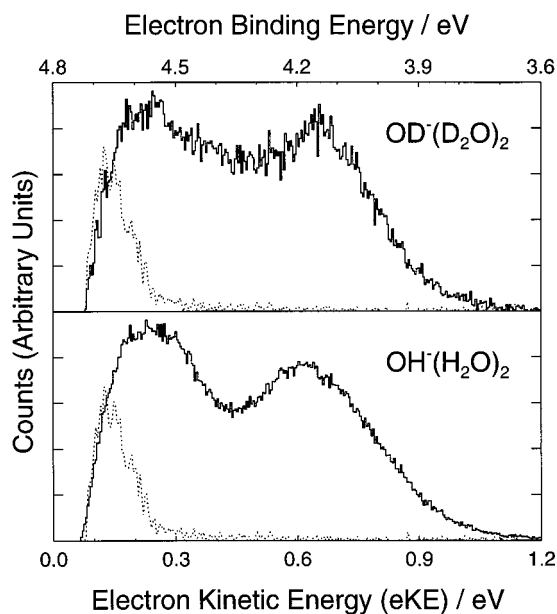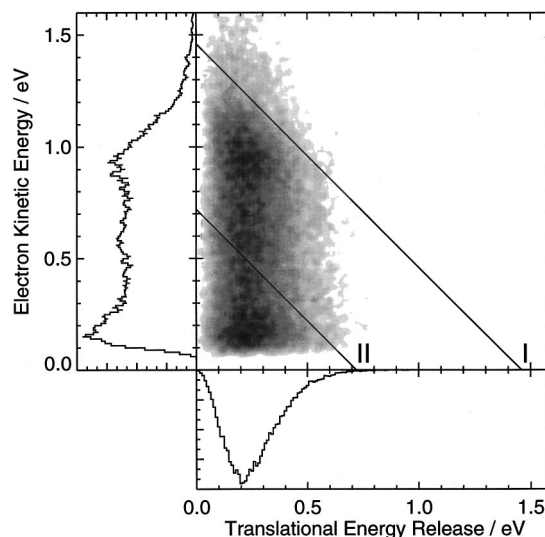
and $OD^-(D_2O)_2$ spectra. At the lower electron kinetic energies, the dotted lines are a measure of the electron background which is primarily a result of the laser beam generating electrons by striking surfaces inside the machine. The broad features observed in both systems are similar to features in the spectra of $O^-(H_2O)$ and $OH^-(H_2O)$,[12,13] except for a shift to lower eKE (higher electron binding energy) owing to the additional solvation energy.

Figures 4 and 5 show the photoelectron–photofragment kinetic energy correlation spectra for $O^-(D_2O)_2$ and $OH^-(H_2O)_2$, respectively. In these plots, the x-axis represents the total photofragment kinetic energy, the y-axis the electron kinetic energy, and the evenly spaced shaded con-

FIG. 3. Photoelectron spectra, $N(\text{eKE})$, of $OH^-(H_2O)_2$ and $OD^-(D_2O)_2$ at 4.8 eV.
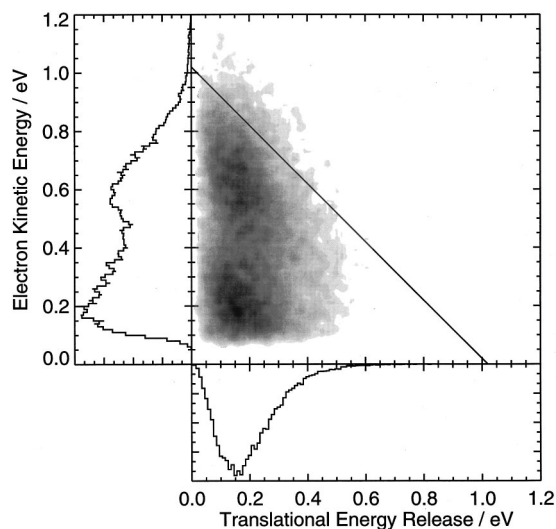

FIG. 5. Photoelectron–photofragment kinetic energy correlation spectrum for $OH^-(H_2O)_2$ at 4.8 eV. The contours represent the number of events with a given correlated value of E_T and eKE, $N(E_T,\text{eKE})$. The diagonal line drawn represents the maximum translational energy, KE_{MAX}, available to the product channel $OH+2H_2O+e^-$.

J. Chem. Phys., Vol. 114, No. 19, 15 May 2001

Studies of O$^-$(H$_2$O)$_2$, OH$^-$(H$_2$O)$_2$ 8439

TABLE I. Peak positions for particle translational energy spectra, $N(E_T)$, of O$^-$(H$_2$O)$_{1,2}$, OH$^-$(H$_2$O)$_{1,2}$, and the deuterated analogs. Uncertainties in the peak positions are ± 0.01 eV.

Molecule	E_T (eV)	ΔE
O$^-$(H$_2$O)[a]	0.11	
O$^-$(H$_2$O)$_2$	0.19	0.08
O$^-$(D$_2$O)[a]	0.14	
O$^-$(D$_2$O)$_2$	0.21	0.07
OH$^-$(H$_2$O)[b]	0.05	
OH$^-$(H$_2$O)$_2$	0.15	0.10
OD$^-$(D$_2$O)[b]	0.12	
OD$^-$(D$_2$O)$_2$	0.18	0.06

[a]Reference 29.
[b]Reference 13.

FIG. 6. Total kinetic energy release spectra, $N(E_{TOT})$, for O$^-$(H$_2$O)$_2$, O$^-$(D$_2$O)$_2$, OH$^-$(H$_2$O)$_2$, and OD$^-$(D$_2$O)$_2$ at 4.8 eV. The data is generated by histogramming the sum $E_{TOT} = E_T + $eKE for each event. The peak positions and spacings are listed in Table II. The dotted vertical line represents KE$_{MAX}$ for each cluster.

tours represent the number of events, $N(E_T,$eKE), with a given correlated electron kinetic energy and photofragment kinetic energy. The $N(E_T)$ and $N($eKE) plots are generated by integrating over the conjugate variable in the $N(E_T,$eKE) spectrum. Spectra for O$^-$(H$_2$O)$_2$ and OD$^-$(D$_2$O)$_2$ are very similar to the spectra shown and are not presented here. The differences in the spectra are the isotope shifts (~ 0.02 eV) and a shift in E_T (see Table I). Unlike the $N(E_T,$eKE) spectra of the singly hydrated species, these spectra show no signs of vibrationally resolved product state distributions.[13] Instead, they contain broad features correlated with the positions of the broad features in the photoelectron spectra.

Using conservation of energy, diagonal lines can be drawn on the correlation spectra corresponding to the maximum translational energy release (KE$_{MAX}$) for different dissociation channels. The rightmost diagonal lines (I) in both Figs. 4 and 5 represent KE$_{MAX}$ for reactions (1) and (3), respectively, where the products are in the lowest quantum states and all excess energy is in translation. Any events that occur below this line are indicative of rovibronic excitation in the products. KE$_{MAX}$ is drawn at the same contour level (15%) as for the singly hydrated system where the position was known based on published thermochemical data.[13] By not including all data within KE$_{MAX}$, the positioning assumes there are some vibrationally excited parent anions which are contributing to the spectrum. This is likely since for O$_3^-$ under similar conditions, vibrational hot bands were seen consistent with vibrational temperatures of 450 K.[48]

In Fig. 4 a diagonal line is drawn (II) for KE$_{MAX}$ of reaction (2). The difference in energy from KE$_{MAX}$(I) is given by the 0 K exoergicity of O+H$_2$O$\rightarrow$2OH.[49] The experimental setup does not have the mass resolution to determine whether events below this energetic limit are from reaction (1) or reaction (2). The ratio of events under KE$_{MAX}$(II) to the total number of events yields an upper limit for the branching ratio of reaction (2) of 35% assuming all events below (II) result from reaction (2).

Figure 6 shows the total kinetic energy ($E_{TOT} = E_T + $eKE) spectra, $N(E_{TOT})$, for all the clusters in this study. These spectra are generated by histogramming the sum of E_T and eKE for each event. Table II lists the peak positions and separations. In our previous studies of the singly hydrated species, a series of peaks appeared in the E_{TOT} spectra corresponding to vibrationally resolved product state distribu-
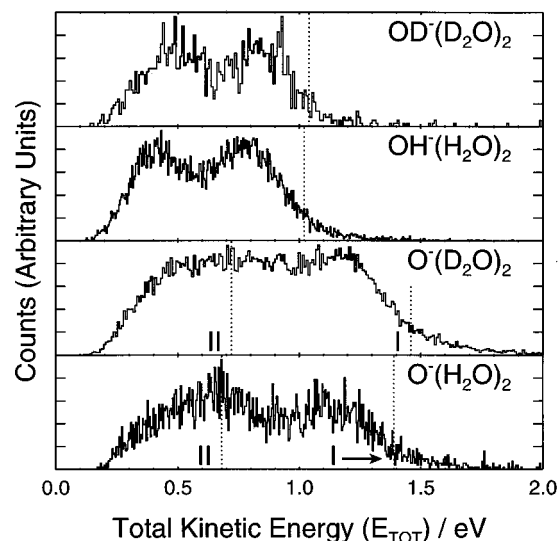
tions with an approximate spacing given by the vibrational frequency of the asymmetric stretch of H$_2$O.[13] In the current spectra these peaks are not observed, presumably due to the higher density of states in the products.

Figure 7 shows the momentum–space molecular frame differential cross section (MF-DCS) for OH$^-$(H$_2$O)$_2$. The generation of these spectra has been described previously.[18] The CM momentum of the lightest particle, OH, is constrained to lie along the x-axis. On an event-by-event basis, the direction and magnitude of the momentum vectors of the two water molecules are plotted relative to the OH neutral, with the faster water molecule plotted in the lower half of the spectrum. Although the $m/\Delta m = 2.5$ mass resolution prevents an unambiguous assignment of OH, Fig. 7 uses the assigned masses for each event as discussed in the experimental section. These plots provide insight into the dynamics of the dissociation event by showing momentum vector correlations between the products. The MF-DCS is only shown for one cluster because the spectra of all four clusters are very similar.

TABLE II. Peak positions and spacing for total energy spectra, $N(E_{TOT})$, of O$^-$(H$_2$O)$_2$, OH$^-$(H$_2$O)$_2$, and the deuterated analogs. Uncertainties in the peak positions are ± 0.04 eV.

Molecule	E_{TOT} (eV)	ΔE
O$^-$(H$_2$O)$_2$	0.67	
	1.12	0.45
O$^-$(D$_2$O)$_2$[a]	0.75	
	1.15	0.40
OH$^-$(H$_2$O)$_2$	0.44	
	0.77	0.33
OD$^-$(D$_2$O)$_2$	0.48	
	0.82	0.33

[a]Positions are only estimates due to the broad nature of the peaks in this spectrum.
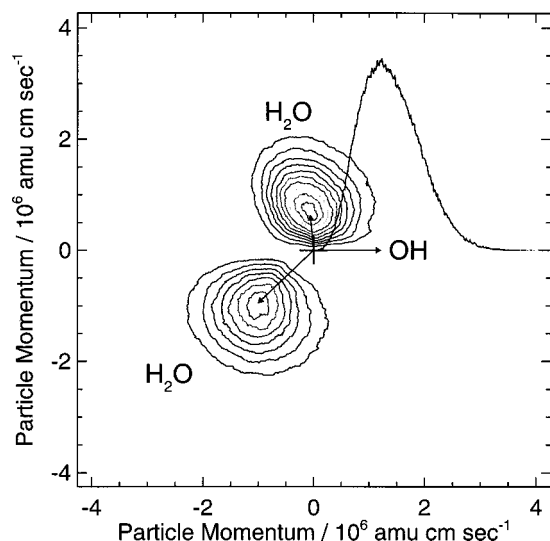
FIG. 7. Momentum-space MF-DCS for $OH(H_2O)_2$. The solid line curve is the distribution of momenta for the particle assigned as OH while the evenly spaced contours represent the distribution of momenta of the two water molecules. The arrows point to the maxima in the distributions of each of the three particles.

Finally, Fig. 8 shows a Dalitz plot for $OH^-(H_2O)_2$. Dalitz plots are commonly employed as a sensitive method to present the dynamics of three-body dissociations.[50–53] The plotting method employed by Wiese *et al.* in their study of H_3^+ is used to construct the figure.[51] A set of coordinates corresponding to the fractional square of the momenta are used. Each axis is given by

$$f(p_i) = p_i^2/(p_1^2 + p_2^2 + p_3^2), \tag{4}$$

where p_i is the momentum of the *i*th particle. For a given event, the location of the plotted point is determined by the value of $f(p_i)$ for each particle, plotted as the perpendicular distance from the side of an equilateral triangle.[54] Due to the choice of coordinates, all events lie inside the triangle which represents conservation of energy. An inscribed circle in the
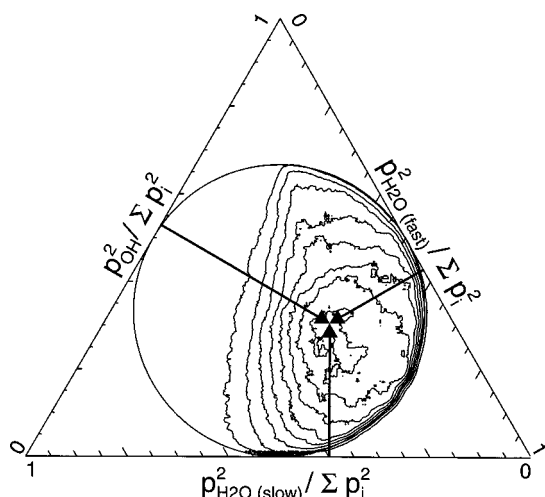

FIG. 8. Dalitz plot representation of the partitioning of the fractional square of the momenta in the three-body dissociative photodetachment $OH^-(H_2O)_2 \rightarrow OH + 2H_2O + e^-$. The arrows point to the centroid of the plot, giving an average distribution among the three neutral fragments.

triangle represents momentum conservation.[55] A Dalitz plot is only shown for $OH^-(H_2O)_2$ because the plots do not differ significantly for the other three complexes studied.

IV. ANALYSIS AND DISCUSSION

The $N(eKE)$ spectra for $O^-(H_2O)_2$ and $O^-(D_2O)_2$ shown in Fig. 2 are qualitatively different from the spectra for the singly hydrated clusters first recorded by Arnold, Xu, and Neumark.[12] All spectra consist of broad features which is expected for clusters with a range of starting geometries, significant internal degrees of freedom, and for molecules which are undergoing dissociation. Lifetime broadening was observed in $O^-(H_2O)$ and $OH^-(H_2O)$ photoelectron spectra[12] and may contribute to the lack of vibrational resolution in the present spectra. In the singly hydrated clusters, isotopic substitution produced a dramatic change in the positions and intensities of the $N(eKE)$ features. In the present case these changes are smaller in magnitude and more difficult to discern due to the broad features. The peak at 0.58 ± 0.02 eV is prominent for $O^-(D_2O)_2$ while it is more of a shoulder for $O^-(H_2O)_2$, obscured by a broad peak at 0.35 ± 0.02 eV. The deuterated spectrum also shows evidence of a peak at 0.19 ± 0.02 eV which is not prominent in the normal spectrum. Using DFT methods Schindler *et al.* calculated that the bond length between the H atom on water and the central O atom in $O^-(H_2O)_{n=1,2}$ increased significantly from the singly to the doubly hydrated cluster ($\Delta R_{H-O} = 0.13$ Å).[24] Calculations at the $UHF/6-311++G^{**}$ level using the GAUSSIAN 94 (Ref. 56) suite of programs yield $\Delta R_{H-O} = 0.08$ Å. The reduced sensitivity to isotopic substitution in the photoelectron spectrum relative to the singly hydrated clusters is consistent with this change in geometry. As the water moves further from the central atom, the H-transfer mode will not dominate the photoelectron spectrum. It is not obvious from the spectra what the active modes are. The many internal degrees of freedom and a wide range of starting geometries may contribute significantly to the widths of the peaks.

The isotopic effects are more subtle in the hydroxide cluster spectra in Fig. 3. As with $O^-(H_2O)_2$, the spectra consist of broad features. In the $OH^-(H_2O)_2$ spectrum the peaks at 0.25 ± 0.02 eV and 0.62 ± 0.02 eV are better resolved than in $OD^-(D_2O)_2$, despite the greater width of the peaks in the $OH^-(H_2O)_2$ spectrum. Perez del Valle and Novoa calculated a relatively flat potential energy surface around the minimum geometry of $OH^-(H_2O)_2$,[36] implying some variation in the anionic starting geometry and therefore a broadening of $N(eKE)$ features. Calculations also predict $\Delta R_{H-O} = 0.12$ Å (Ref. 34) for $OH^-(H_2O)_2$. As suggested previously, the reduced sensitivity of the $N(eKE)$ spectra to isotopic substitution is consistent with this geometry change. Here as with the $O^-(H_2O)_2$ clusters there is a slight shift to higher eKE upon deuteration. This shift must derive from a larger zero point energy stabilization of the neutral products over the anionic precursor upon deuteration.

The larger isotopic dependence of the oxide cluster spectrum was also evident in the singly hydrated cluster data where the relative contributions of the assigned photoelectron peaks altered more significantly for $O^-(H_2O)$ than

$OH^-(H_2O)$.[12] These spectral changes were due to a shift in the harmonic frequencies upon isotopic substitution which altered the Franck–Condon overlap between the anionic and neutral wave functions. Franck–Condon factor (FCF) calculations could be employed to simulate the photoelectron spectra and determine the active modes of the doubly hydrated clusters. Owing to the difficult nature of accurate calculations on these systems, especially on the open-shell oxide clusters, FCF calculations are beyond the scope of this paper.

Additional information can be obtained concerning the charge distribution within the anion by comparing the spectra of the oxide and hydroxide clusters. An energetic shift of 0.32 eV is found by extrapolating the trailing edges in the $O^-(H_2O)_2$ and $OH^-(H_2O)_2$ photoelectron spectra. The difference in the electron affinities of O and OH is 0.36 eV. The similarity of these values implies that most of the charge in the molecule resides on the central moiety, and is not significantly transferred to the solvent molecules. For the same type of extrapolation on the singly hydrated molecules, the difference is only 0.23 eV. These observations imply that the features in the photoelectron spectra are more closely related to the spectra of the central moiety than in the singly hydrated case and are consistent with the theoretical calculations of Grimm *et al.* who reported increasing localization of charge on the hydroxide center with increasing hydration.[41]

Table 1 lists the peak positions in the $N(E_T)$ spectra for $O^-(H_2O)_{n=1,2}$, $OH^-(H_2O)_{n=1,2}$, and the deuterated analogs. In all cases, the deuterated clusters showed a higher E_T than the normal clusters, and the doubly hydrated clusters showed a higher E_T than the singly hydrated clusters. In studies of $OH^-(H_2O)$ and $OD^-(D_2O)$, Deyerl *et al.* attributed the former effect to the lower zero point energy of the deuterated species, which led to a contraction of the anion wave function and yielded a larger Franck–Condon overlap with more repulsive regions of the neutral potential surface upon photodetachment.[13] For OH^-, E_T increases by 0.1 eV from the singly to the doubly hydrated cluster. Addition of a second water to O^- and OH^- might be expected to decrease E_T since it is generally expected that additional degrees of freedom would lead to distribution of energy into these degrees of freedom in the dissociation.

The counterintuitive increase in E_T may be due to the geometry of the cluster, however. As mentioned previously, $OH^-(H_2O)_2$ is the only species which has been extensively studied theoretically. The geometry of the cluster shown in Fig. 1(c) is determined by the strong hydroxide ion–water interaction and exhibits a marked water–water repulsion of 0.48 eV.[34] This large repulsion could account for the larger E_T observed in the two-water system. Immediately after photodetachment, the neutral cluster is in the anion configuration, and the water molecules may retain the large repulsion induced by the stronger intracluster bonding in the anion. At best, the neutral cluster is weakly bound in the van der Waals geometry, and at the anionic geometry the large water–water repulsion may force the cluster apart with a large E_T.

Since high-level *ab initio* geometries and energies do not exist for $O^-(H_2O)_2$, it is difficult to make a direct comparison between $O^-(H_2O)_2$ and $OH^-(H_2O)_2$. The previously mentioned UHF calculations indicate that the geometry of $O^-(H_2O)_2$ is essentially linear, as shown in Fig. 1(b), while calculations for $OH^-(H_2O)_2$ at the same level of theory place the O–O–O bond angle at 124.5°, similar to that in Fig. 1(c). In a linear geometry, the water–water repulsion in $O^-(H_2O)_2$ is expected to be smaller, yielding E_T distributions peaked at lower energies relative to $OH^-(H_2O)_2$. This trend is not observed in the data, however. The change in E_T upon addition of a second water to the $O^-(H_2O)$ is comparable to that of $OH^-(H_2O)$ (and their deuterated analogs) which emphasizes the need for high-level *ab initio* calculations on this difficult open shell species to aid in explaining the observed increase in E_T.

The $N(E_T,eKE)$ spectra also provide information about the dynamics of dissociative photodetachment. In the singly hydrated clusters, these spectra revealed vibrationally resolved translational energy distributions as diagonal bands in the spectra. Diagonal bands are not observed in the correlation spectra for the doubly hydrated species, nor is there any correlation between E_T and eKE beyond conservation of energy as can be seen from the vertical shape of the spectra. A lack of correlation between E_T and eKE may imply that the photodetachment and dissociation events are occurring on different time scales due to a long-lived neutral intermediate allowing redistribution of energy after photodetachment. The neutral intermediate lifetime will be discussed further when the MF-DCS and Dalitz plots of the three-body dynamics are discussed.

The maximum energy released in translation, KE_{MAX}, can be used to calculate previously undetermined values for $\Delta E^{hyd}_{0\,K,1\leftarrow2}(O^-)$ with both water and deuterated water. $\Delta H^{hyd}_{298\,K,1\leftarrow2}(OH^-)$ for both the normal and deuterated species are already known through several experiments.[19,42–44] $\Delta E^{hyd}_{0\,K,1\leftarrow2}(O^-)$ is determined by using the energetic relationships between KE_{MAX}, the electron affinity of atomic oxygen [EA(O)], and $\Delta E^{hyd}_{0\,K,0\leftarrow1}(O^-)$ as shown in Fig. 9(a). For normal and deuterated O and OH, $\Delta E^{hyd}_{0\,K,0\leftarrow1}$ has been measured in this laboratory.[13,29] In order to compare this data with experimental values of hydration energies, the 0 K value needs to be corrected to 298 K. This was done for the present systems by estimating the vibrational contribution to the heat capacity for the hydration reaction,[57] yielding the values of $\Delta H^{hyd}_{298\,K,1\leftarrow2}$ listed in Table III along with several values from previous experiments and theoretical calculations. The low frequency modes of the clusters provide a significant portion of the vibrational heat capacity correction. Although the frequencies of these modes are difficult to calculate accurately, the direction of the correction is consistent with the larger number of low frequency vibrational modes in the dimer clusters compared to the monomer clusters. The overall correction is on the order of the uncertainty in the 0 K energy and owing to this small magnitude, the uncertainty in $\Delta H^{hyd}_{298\,K,1\leftarrow2}$ should not be significantly affected.

There are no experimental reports of $\Delta H^{hyd}_{298\,K,1\leftarrow2}(O^-)$ for comparison with the present results. The present value of 0.78 ± 0.06 eV for $\Delta E^{hyd}_{0\,K,1\leftarrow2}(OH^-)$, temperature corrected to $\Delta H^{hyd}_{298\,K,1\leftarrow2}(OH^-)=0.70\pm0.06$ eV, compares favorably to the previous determinations of 0.71–0.78 eV (at 298 K). At first glance, the trends found in the second hydration en-
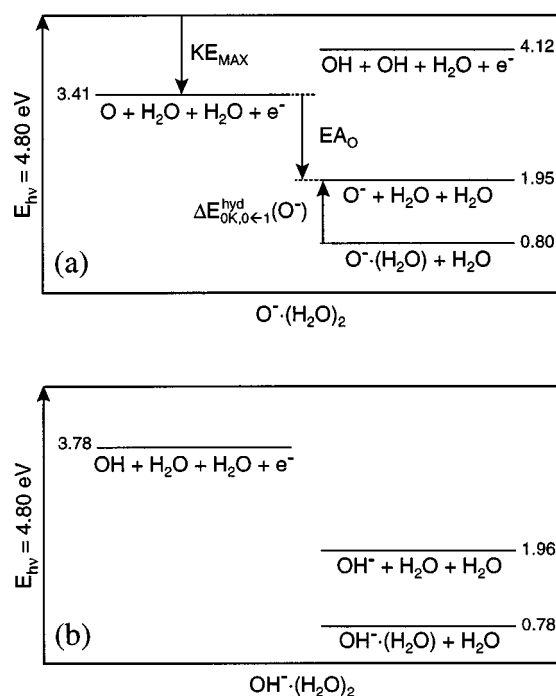
FIG. 9. Energetics diagram for (a) $O^-(H_2O)_2$ and (b) $OH^-(H_2O)_2$ showing the dissociative photodetachment and ionic dissociation processes relevant to determining the incremental hydration energies as discussed in the text.

ergies are surprising. The normal and deuterated $\Delta E_{0\ K,1\leftarrow2}^{hyd}(O^-)$ differ by only 0.01 eV, while for hydroxide the difference is 0.13 eV. It is surprising to find a large difference in $\Delta E_{0\ K,1\leftarrow2}^{hyd}(OH^-)$ upon deuteration while $\Delta E_{0\ K,1\leftarrow2}^{hyd}(O^-)$ remains essentially constant. $\Delta E_{0\ K,0\leftarrow1}^{hyd}(OH^-)$ also changed significantly upon deuteration, primarily as a result of the difference in heats of formation between the two anions.[13] In the present case, the difference in heats of formation can be calculated by using the 0 K heat of formation of OH/OD,[49] the electron affinity of OH/OD,[58] and the incremental hydration energies of

OH (Ref. 43) and OD (Ref. 42) (corrected to 0 K using the estimated vibrational contributions as discussed above). This gives a difference in heats of formation of $\Delta(\Delta_f E_{0\ K})(OD^-(D_2O)_2 - OH^-(H_2O)_2) = 0.144 \pm 0.09$ eV which yields $\Delta KE_{MAX} = 0.14 \pm 0.09$ eV. The uncertainty in $\Delta(\Delta_f E_{0\ K})$ was estimated since uncertainties were not given in the original papers. The estimated ΔKE_{MAX} matches quite well with the experimentally observed difference of 0.13 eV, thus the surprise lies more in the agreement of the oxide energies rather than in the difference in the hydroxide energies. Similar incremental hydration energy data is not available for the oxide compound, and a ΔKE_{MAX} estimation cannot be made.

Finally, the MF-DCS in Fig. 7 and the Dalitz plot in Fig. 8 provide insights into the dissociation dynamics of $OH(H_2O)_2$ and the other clusters studied here. Measurement of the time- and position-of-arrival of all particles in coincidence yields a kinematically complete description of the dissociation. The nomenclature proposed by Maul and Gericke for synchronous concerted, asynchronous concerted and sequential reaction mechanisms is used in the following discussion.[59] In the case of a synchronous concerted three-body breakup from a range of geometries, measurement of the three momenta would provide a distinctly shaped MF-DCS and would be represented on a Dalitz plot by a straight line. In the case of the present clusters these signatures are not observed, implying an asynchronous concerted or sequential mechanism.

In Figs. 7 and 8, the data show a wide distribution of momenta among the three particles. This is in contrast to O_6^-, where two of the particles carried most of the momentum, and the third particle acted as a spectator.[60] In the three-body dissociative photodetachment $O_3^-(D_2O) + h\nu \rightarrow O + O_2 + D_2O + e^-$, it was found that the heaviest product, O_2, received most of the momentum.[18] From the MF-DCS for $OH^-(H_2O)_2$, on average two molecules receive approximately 40% of the total momentum each and the third mol-

TABLE III. Second hydration energies for O^- and OH^- and the deuterated analogs.

Molecule	Method[a]	Ref.	$\Delta E_{0\ K,1\leftarrow2}$ (eV)	$\Delta H_{298\ K,1\leftarrow2}$ (eV)
$O^-(H_2O)_{n,n-1}$	PPC	this work	0.80 ± 0.08	0.71 ± 0.08^b
	analogy to OH series	19		0.74
	LSD+BP/DZVP2[c]	24		0.83
$O^-(D_2O)_{n,n-1}$	PPC	this work	0.81 ± 0.08	0.71 ± 0.08^b
$OH^-(H_2O)_{n,n-1}$	PPC	this work	0.78 ± 0.06	0.70 ± 0.06^b
	HPMS	43		0.78
	HPMS	44		0.76
	LDF+BP/DZVP2[c]	24		0.77
	MP2/aug-cc-pvdz	34		0.87
	BLYP/aug-cc-pvdz	36		0.81
	MP4/6-311+G(2df,2p)	38		0.87
$OD^-(D_2O)_{n,n-1}$	PPC	this work	0.91 ± 0.06	0.82 ± 0.06^b
	MS	45		1.00
	HPMS	42		0.71
	MP4/6-311+G(2df,2p)	38		0.89

[a]PPC: Photoelectron–photofragment coincidence spectroscopy. HPMS: high-pressure mass spectrometry. MS: mass spectrometry.
[b]Correction of the measured 0 K energy to the 298 K enthalpy was performed as discussed in the text.
[c]See Ref. 24 for a description of these methods.

ecule receives the remaining 20% of the momentum. Examining the centroids of the distributions, the MF-DCS and Dalitz plots yield slightly different values for the average momentum partitioning among the three particles. This is a result of the lack of correlation in the MF-DCS; the three centroids do not necessarily correspond to momentum partitioning in actual events, but are instead the average momentum, independently determined for each particle. However, the single centroid of the distributions in the Dalitz plot corresponds directly to the most probable momentum distribution for the three particles in an event. The three momenta are also very broadly distributed, both in the total momentum transferred to each particle and in the angles between the momenta of the particles. Broad momentum partitioning consistent with the MF-DCS is also seen in the Dalitz plot. In Fig. 8, the data covers half of the phase space of the plot, with a slight concentration towards the lower right portion of the plot. The broad momentum distributions imply that the dissociation reaction is either not instantaneous or does not occur from a well-defined initial geometry. The data is consistent with a mechanism where the photodetached anion has a distribution of starting geometries and one water molecule, likely the fast water molecule, dissociates quickly after photodetachment leaving a OH(H$_2$O) intermediate which subsequently dissociates, yielding the hydroxyl radical and the second water molecule.

V. CONCLUSIONS

Photoelectron–photofragment coincidence spectroscopy was employed to study the energetics and three-body dissociative photodetachment dynamics of O$^-$(H$_2$O)$_2$, OH$^-$(H$_2$O)$_2$, and the deuterated isotopomers. The 0 K second incremental hydration/dissociation energies, $\Delta E_{0\,K,1\leftarrow2}^{hyd}$, are reported for all four anions. They are found to be 0.80 $\pm$0.08, 0.81$\pm$0.08, 0.78$\pm$0.06, and 0.91$\pm$0.06 eV for normal O$^-$, deuterated O$^-$, normal OH$^-$, and deuterated OD$^-$, respectively. The results for $\Delta E_{0\,K,1\leftarrow2}^{hyd}$(O$^-$) are the first reported experimental values for this quantity. The hydration energy for OH$^-$(H$_2$O)$_2$ is consistent with previous experiments after taking into account estimated corrections from vibrational contributions to the heat capacity at 298 K.

The photoelectron and total kinetic energy spectra from these systems exhibit isotopic dependence, with variations in peak intensity and position upon deuteration. These changes are more prevalent in the oxide system than the hydroxide system. The spectral variations are consistent with the changes in the singly hydrated clusters,[12,13] and can be attributed to a convolution of effects arising from the change in density of states and Franck–Condon overlap upon deuteration. The effects of isotopic substitution are less predominant than in the singly hydrated clusters, most likely arising from the increased degrees of freedom, larger distance between the central moiety and the water molecules, as well as the increased localization of the charge on the central moiety.

All four clusters are found to have very similar dissociation dynamics despite the differences in energetics caused by the different central moiety. The data is consistent with photodetachment from a wide range of anionic geometries followed by the creation of an intermediate neutral cluster consisting of an oxygen or hydroxyl radical and a water molecule which subsequently undergoes dissociation. The kinetic energy release of each of the doubly hydrated clusters was found to exceed that of the singly hydrated. This observation is consistent with a large water–water repulsion that has been calculated for OH$^-$(H$_2$O)$_2$ as well as a weakened water–hydroxide bond in the doubly hydrated cluster. High-level *ab initio* calculations on O$^-$(H$_2$O)$_2$, although difficult due to the open-shell nature of the clusters, would permit evaluation of the extent to which a geometry change in the anion effects the dissociative photodetachment dynamics. The data provided by these experiments will be useful as a test for future high-level structural and dynamical calculations.

[1] F. Arnold, J. Kissel, D. Krankowsky, H. Wieder, and J. Zähringer, J. Atmos. Terr. Phys. **33**, 1169 (1971).
[2] R. S. Narcisi, A. D. Bailey, L. Della Lucca, C. Sherman, and D. M. Thomas, J. Atmos. Terr. Phys. **33**, 1147 (1971).
[3] *Atmospheric Water Vapor*, edited by A. Deepak, T. D. Wilkerson, and L. H. Ruhnke (Academic, New York, 1980).
[4] A. A. Viggiano and F. Arnold, in *Atmospheric Electrodynamics*, edited by H. Volland (CRC Press, Boca Raton, 1995), pp. 1–25.
[5] P. F. Knewstubb and T. M. Sugden, Nature (London) **196**, 1311 (1962).
[6] R. Atkinson, Chem. Rev. **86**, 69 (1986).
[7] H. G. Tremmel, H. Schlager, P. Konopka, P. Schulte, F. Arnold, M. Klemm, and B. Droste-Franke, J. Geophys. Res., [Atmos.] **103**, 10803 (1998).
[8] S. Böckle, S. Einecke, F. Hildenbrand, C. Orlemann, C. Schulz, J. Wolfrum, and V. Sick, Geophys. Res. Lett. **26**, 1849 (1999).
[9] S. A. McKeen, G. Mount, F. Eisele, E. Williams, J. Harder, P. Goldan, W. Kuster, S. C. Liu, K. Baumann, D. Tanner, A. Fried, S. Sewell, C. Cantrell, and R. Shetter, J. Geophys. Res., [Atmos.] **102**, 6467 (1997).
[10] M. K. Dubey, R. Mohrschladt, N. M. Donahue, and J. G. Anderson, J. Phys. Chem. A **101**, 1494 (1997).
[11] U. K. Kläning, E. Larsen, and K. Sehested, J. Phys. Chem. **98**, 8946 (1994).
[12] D. W. Arnold, C. Xu, and D. M. Neumark, J. Chem. Phys. **102**, 6088 (1995).
[13] H.-J. Deyerl, A. K. Luong, T. G. Clements, and R. E. Continetti, Faraday Discuss. **115**, 147 (2000).
[14] R. G. Keesee, N. Lee, and A. W. Castleman, Jr., J. Chem. Phys. **73**, 2195 (1980).
[15] J. V. Coe, Chem. Phys. Lett. **229**, 161 (1994).
[16] F. C. Fehsenfeld and E. E. Ferguson, J. Chem. Phys. **61**, 3181 (1974).
[17] R. E. Continetti, Int. Rev. Phys. Chem. **17**, 227 (1998).
[18] A. K. Luong, T. G. Clements, and R. E. Continetti, J. Phys. Chem. A **103**, 10237 (1999).
[19] A. A. Viggiano, R. A. Morris, C. A. Deakyne, F. Dale, and J. F. Paulson, J. Phys. Chem. **94**, 8193 (1990).

[20] X. Yang and A. W. Castleman, J. Phys. Chem. **95**, 6182 (1991).

[21] X. Yang, X. Zhang, and A. W. Castleman, J. Phys. Chem. **95**, 8520 (1991).

[22] A. A. Viggiano, R. A. Morris, C. A. Deakyne, F. Dale, and J. F. Paulson, J. Phys. Chem. **95**, 3644 (1991).

[23] X. Yang and A. W. Castleman, J. Am. Chem. Soc. **113**, 6766 (1991).

[24] T. Schindler, C. Berg, G. Niedner-Schatteburg, and V. E. Bondybey, J. Phys. Chem. **99**, 12434 (1995).

[25] H. Wincel, E. Mereand, and A. W. Castleman, J. Phys. Chem. **100**, 16808 (1996).

[26] E. Mereand, H. Wincel, and A. W. Castleman, Int. J. Mass. Spectrom. **182/183**, 31 (1999).

[27] J. K. Labanowski and J. W. Andzelm, *Density Functional Methods in Chemistry* (Springer, New York, 1991).

[28] J. Andzelm and E. Wimmer, J. Chem. Phys. **96**, 1280 (1992).

[29] H. J. Deyerl and R. E. Continetti (in preparation).

[30] P. M. Hierl and J. F. Paulson, J. Chem. Phys. **80**, 4890 (1984).

[31] X. Yang and A. W. J. Castleman, J. Phys. Chem. **94**, 8500 (1990).

[32] M. D. Newton and S. Ehrenson, J. Am. Chem. Soc. **93**, 4971 (1971).

[33] A. M. Sapse, L. Osorio, and G. Snyder, Int. J. Quantum Chem. **26**, 223 (1984).

[34] S. S. Xantheas, J. Am. Chem. Soc. **117**, 10373 (1995).

[35] J. J. Novoa, F. Mota, C. Perez del Valle, and M. Planas, J. Phys. Chem. A **101**, 7842 (1997).

[36] C. Perez del Valle and J. J. Novoa, Chem. Phys. Lett. **269**, 401 (1997).

[37] N. Turki, A. Milet, A. Rahmouni, O. Ouamerali, R. Moszynski, E. Kochanski, and P. E. S. Wormer, J. Chem. Phys. **109**, 7157 (1998).

[38] J. R. Pliego and J. M. Riveros, J. Chem. Phys. **112**, 4045 (2000).

[39] A. Vegiri and S. V. Shevkunov, J. Chem. Phys. **113**, 8521 (2000).

[40] I. Tuñón, D. Rinaldi, M. F. Ruiz-López, and J. L. Rivail, J. Phys. Chem. **99**, 3798 (1995).

[41] A. R. Grimm, G. B. Bacskay, and A. D. J. Haymet, Mol. Phys. **86**, 369 (1995).

[42] M. Arshadi and P. Kebarle, J. Phys. Chem. **74**, 1483 (1970).

[43] J. D. Payzant, R. Yamdagni, and P. Kebarle, Can. J. Chem. **49**, 3308 (1971).

[44] M. Meot-Ner and C. V. Speller, J. Phys. Chem. **90**, 6616 (1986).

[45] M. De Paz, A. G. Giardini, and L. Friedman, J. Chem. Phys. **52**, 687 (1970).

[46] K. A. Hanold, A. K. Luong, T. G. Clements, and R. E. Continetti, Rev. Sci. Instrum. **70**, 2268 (1999).

[47] K. A. Hanold, A. K. Luong, and R. E. Continetti, J. Chem. Phys. **109**, 9215 (1998).

[48] M. C. Garner, K. A. Hanold, M. S. Resat, and R. E. Continetti, J. Phys. Chem. A **101**, 6577 (1997).

[49] M. W. Chase, Jr., C. A. Davies, J. R. Downy, Jr., D. J. Frurip, R. A. McDonald, and A. N. Syverud, *JANAF Thermochemical Tables*, Suppl. 1 ed. (American Institute of Physics, New York, 1985).

[50] R. H. Dalitz, Philos. Mag. **44**, 1068 (1953).

[51] L. M. Wiese, O. Yenen, B. Thaden, and D. H. Jaecks, Phys. Rev. Lett. **79**, 4982 (1997).

[52] U. Müller, T. Eckert, M. Braun, and H. Helm, Phys. Rev. Lett. **83**, 2718 (1999).

[53] C. Maul and K. H. Gericke, J. Phys. Chem. A **104**, 2531 (2000).

[54] Owing to our inability to distinguish the masses of the products, threefold rotation symmetry and mirror symmetry with respect to the perpendiculars of each edge of the equilateral triangle should be imposed (Ref. 52). However, in order to be consistent with the plotting order of the MF-DCS, the Dalitz plot uses the same assignments for the fragments as was employed in Fig. 7.

[55] R. Hagedorn, *Relativistic Kinematics: A Guide to the Kinematic Problems of High-Energy Physics* (Benjamin, New York, 1963).

[56] M. J. Frisch, G. W. Trucks, H. B. Schlegel *et al.*, GAUSSIAN 94, Revision E.2 (Gaussian, Inc., Pittsburgh, PA, 1995).

[57] The integrated contributions to the vibrational heat capacity were derived from either scaled calculated or experimental vibrational frequencies. For example, the 298 K correction to the 0 K second hydration energy of oxide was based on the correction for each species in the reaction $O^-(H_2O)_2 \rightarrow O^-(H_2O) + H_2O$. For all the calculations, the 6-311++G** basis set was employed, varying only in the method, UHF for $O^-(H_2O)_2$ and $O^-(H_2O)$, and MP2 for $OH^-(H_2O)_2$ and $OH^-(H_2O)$. The calculations on the deuterated molecules used the same method as the normal molecule. For H_2O/D_2O, experimental vibrational frequencies were employed.

[58] P. A. Schulz, R. D. Mead, P. L. Jones, and W. C. Lineberger, J. Chem. Phys. **77**, 1153 (1982).

[59] C. Maul and K.-H. Gericke, Int. Rev. Phys. Chem. **16**, 1 (1997).

[60] A. K. Luong, T. G. Clements, and R. E. Continetti, in *Imaging in Chemical Dynamics*, edited by A. G. Suits and R. E. Continetti (American Chemical Society, Washington, D.C., 2001), pp. 312–325.